Development of a flat-field grazing-incidence XUV spectrometer and its application in picosecond XUV spectroscopy

Noboru Nakano, Hiroto Kuroda, Toshiaki Kita, and Tatsuo Harada

A new type of grazing-incidence spectrometer with a flat focal field is developed, and XUV spectroscopy in the extreme ultraviolet region ranging from 15 to 200 Å is carried out. Soft x-ray line spectra emitted from picosecond laser plasmas of aluminum and iron targets are measured and good resolutions are obtained in the XUV region. The spectral regions of detection are extended to shorter wavelengths (15 Å) using a finer spaced grating. Computational studies on x-ray spectra are also performed taking into account the transient characteristics of picosecond laser-produced plasmas; the importance of the transient treatment is clearly shown. This type of soft x-ray spectrometer should be useful for time-resolved picosecond soft x-ray spectroscopy.

I. Introduction

A number of theoretical and experimental studies of low-density plasmas (such as tokamak plasmas) and also of high-density plasmas (such as laser-produced plasmas) have been carried out to study their applications to nuclear fusion. Many spectroscopic measurements of x rays emitted from plasmas have been performed because x-ray spectra offer us much important information without disturbing the host plasma such as temperatures and densities of plasmas and characteristic species of impurities. In addition, advanced spectroscopy in the extreme ultraviolet region, which includes the soft x-ray region (the XUV region), is necessary in physics, chemistry, and biology research.

In the short-wavelength region below 200–300 Å, grazing-incidence mounts are used to increase the reflectivity of the grating surface. With conventional spectrometers, spectra are focused on the Rowland circle with large astigmatism, so that precise setting and positioning of a photographic plate are not easy. A flat focal plane is desirable for various kinds of detector equipped with plane photosensitive surfaces such as microchannel plates (MCP) and streak cameras. Thus, 2-D data processing will be easily performed with the aid of 2-D detectors.

Recently, Fonck *et al.*[1] developed a grazing-incidence spectrometer that uses a holographic grating with flat focal fields for plasma diagnosis. Their spectrometer provides two interchangeable aberration-corrected toroidal gratings to cover the 100–1100- and 160–1700-Å wavelength ranges. However, the position of the focal plane and the resolution of the spectral images are limited by the holographic groove arrangement. We reported an XUV spectrometer with a flat-field focal plane using a grating equipped with mechanically ruled varied pitches (average pitch 1200 grooves/mm)[2] with preliminary results of measurements of XUV spectra emitted from carbon and aluminum plasmas. The advantage of a mechanically ruled aberration-corrected grating is that image focusing can be optimized for the optical arrangement by numerical control of the groove spacing.

The purpose of this paper is to describe various characteristics of the flat-field XUV spectrometer and to show that this spectrometer has many advantages over the conventional instrument. First, we demonstrate how clearly XUV spectra emitted from picosecond laser-produced plasmas can be measured and recorded on a conventional flat photographic plate; we also evaluate characteristic parameters such as spectral resolution when gratings with average ruled pitches of 1200 and 2400 grooves/mm are used. Second, we show that the detection limit toward shorter wavelengths of this spectrometer is extended to ~15 Å with a 2400-grooves/mm grating. Finally, we show the main char-

T. Kita and T. Harada are with Hitachi, Ltd., Central Research Laboratory, Kokunbunji, Tokyo 185, Japan; the other authors are with University of Tokyo, Institute for Solid State Physics, Roppongi, Minato-ku, Tokyo 105, Japan.

Received 5 January 1984.
0003-6935/84/142386-07$02.00/0.

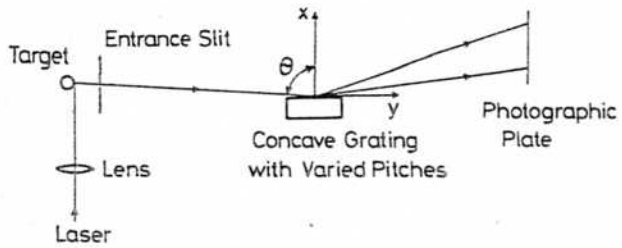

Fig. 1. Schematic and design specifications of the flat-field spectrometer.

acteristic results of measurements of picosecond XUV spectra generated from picosecond laser-produced plasmas with this new type of spectrometer. We also performed computational studies and we show that experimentally observed spectra can be explained when transient dynamical processes associated with the x-ray generation from laser plasmas are taken into account.

II. Experiments and Results

Figure 1 is a schematic diagram showing how to measure XUV spectra from laser-produced plasmas. Laser plasmas produced by a picosecond laser are considered the most desirable calibration sources in the XUV and soft x-ray region, because picosecond laser-produced plasmas are not obscured by the hydrodynamic expansion inherent in other light sources with longer pulse times. The spectrometer is coupled to a diffusion pump and evacuated to 10^{-6} Torr. A YAG laser system equipped with four amplifiers is used for plasma production.[3,4] A single pulse switched out of a mode-locked pulse train is amplified to 200 mJ with a 30-psec pulse duration and focused on a target sustained in vacuum using a lens with a 100-mm focal length. The performance of a mechanically ruled aberration-corrected concave grating with average spacing of 1/1200 mm, 5649-mm radius, and 50- × 30-mm^2 ruled area used for this spectrometer is presented in Ref. 5. Calculated focal curves using the incidence angle as a parameter for gratings with 1200 and 2400 grooves/mm are shown in Figs. 2(a) and (b), respectively. The focal condition is varied abruptly with the varying incident angles. The incident angles for a grating with 1200 grooves/mm and 2400 grooves/mm are 87° and 89°, respectively. For precise adjustment of the incident angle, the grating is mounted on a goniometer and the angular position of the grating is carefully adjusted until sharpness of the x-ray lines ranging over the full spectral region is obtained. For adjusting the focal position, a photographic plate holder is mounted on a rotary table and an X–Y stage. These adjustments can be easily performed from outside the spectrometer. In the present experiment, both Polaroid film (Type 107) and x-ray film (Kodak *No* Screen) are used as photographic plates.

Typical soft x-ray line spectra emitted from laser plasmas of aluminum and iron targets, obtained with this grazing-incidence spectrometer, are shown in Figs. 3(a) and (b). These spectra were obtained by accumulating signals produced by 100 shots of the YAG laser. As is clear in the spectrum taken by the 2400-

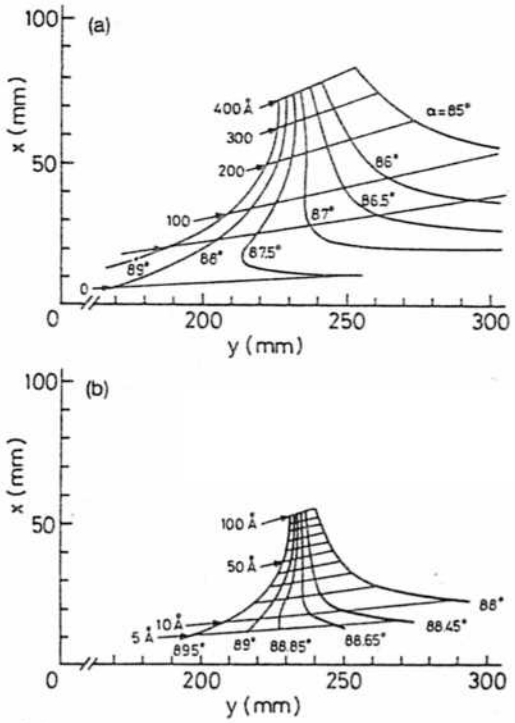

Fig. 2. Calculated focal curves of the aberration-corrected concave grating using the incidence angle as a parameter. The distance between grating center and entrance slit is 237 mm. (a) For a 1200-grooves/mm grating. (b) For a 2400-grooves/mm grating.

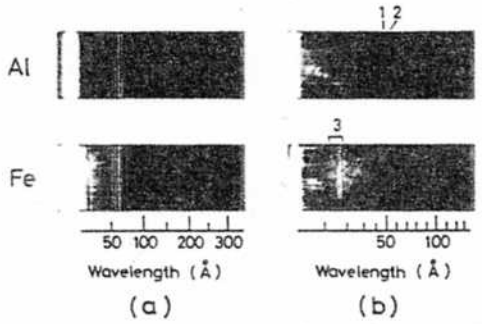

Fig. 3. Typical soft x-ray line spectra obtained on x-ray films. (a) and (b) show the spectra from laser-produced plasmas by using gratings with 1200 and 2400 grooves/mm, respectively, for an aluminum target and an iron target.

grooves/mm grating shown in Fig. 3(b), x-ray lines down to ~15 Å are clearly observed. From this it was concluded that an extension of the detection limit toward the shorter wavelength region can be successfully achieved by adopting the new 2400-grooves/mm grating. Figures 4(a) and (b) show densitometer traces of iron spectra measured with a 1200-grooves/mm grating and a 2400-grooves/mm grating. It is clear that the reflectivity of a 2400-grooves/mm grating is lower than that of a 1200-grooves/mm grating in the longer wavelength region over 100 Å.

III. Computations and Results

A. Basic Equations

For spectroscopy in the soft x-ray and XUV regions, synchrotron orbital radiation (SOR) and emissions from

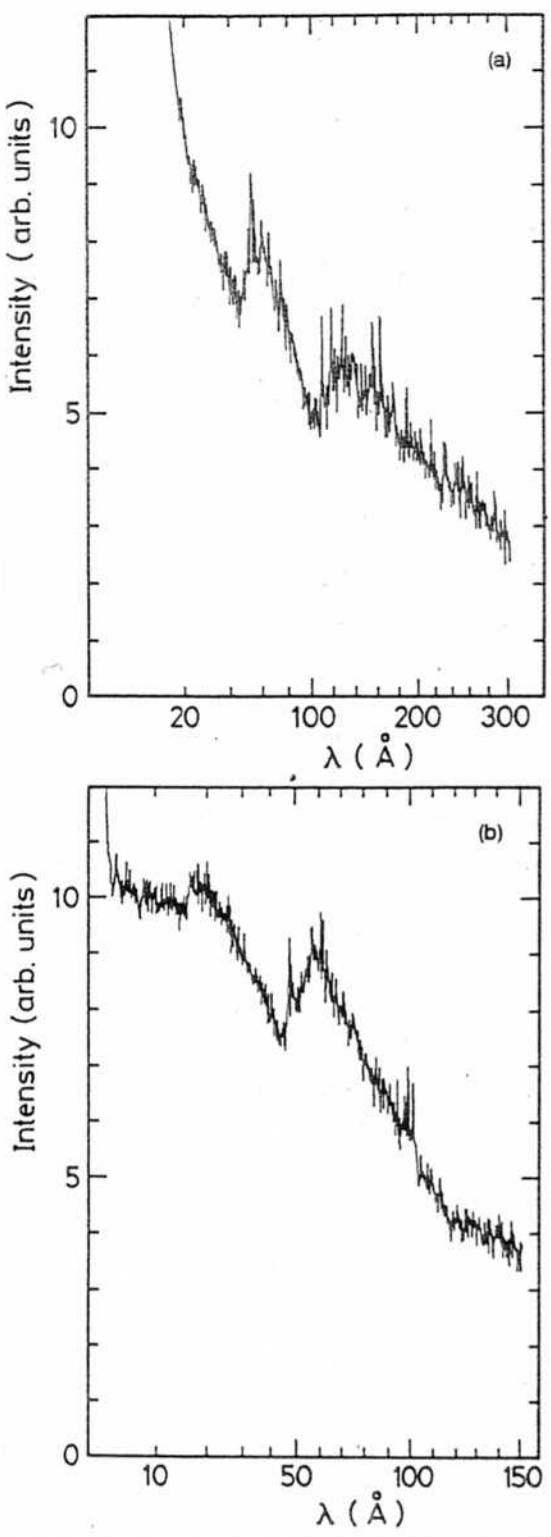

Fig. 4. Microdensitometer traces of photographic plates. (a) and (b) indicate results for gratings with 1200 and 2400 grooves/mm, respectively.

a gas-discharge tube and laser plasmas have been used as light sources. Because of the large facilities installed for the SOR system, experiments using this system cannot be easily performed. Spectra from a gas discharge in a tube filled, for example, with helium gas are limited to the wavelength regions down to 300 Å at the shortest wavelengths. Laser plasmas have an advantage that in their emission spectra short-wavelength components near several angstroms are observed, also laser systems using x-ray spetroscopy are not large enough to be easily operated. In addition, laser plasmas have another advantage: that the area of the emission region is determined by the focused area of the laser beam and, therefore it can be safely regarded as a point source. These light sources are also useful as calibration sources for measuring resolutions, reflectances, and transfer functions of x-ray spectrometers. Theoretical and computational studies of x rays emitted from laser plasmas are necessary to utilize laser plasmas as standard calibrating sources in XUV regions. So far, almost all theoretical analyses are based on the steady-state model, and the dynamic characteristics associated with x-ray and XUV radiation remain to be clarified. For these studies, the transient characteristics of laser plasmas must be considered including the dynamic atomic processes which play an important role in producing highly excited, ionized plasmas.

B. Computational Results

For making computations of picosecond XUV radiation emitted from picosecond laser-produced plasmas, we use the computational model described in Ref. 3. The following equations are solved:

$$dn_j/dt = n_e[n_{j+1}\,\alpha_j - n_j[S_j + \alpha_{j-1}] + n_{j-1}S_{j-1}], \quad 0 \le j \le z, \tag{1}$$

where

$$\alpha_{-1} = S_{-1} = \alpha_Z = S_Z = 0,$$

$$\alpha_j = \beta_{j,r} + n_e\,\beta_{j,3b},$$

$$S_j = 9 \times 10^{-6}\,\xi_j(T_e/\chi_j)^{1/2}\exp(-\chi_j/T_e)/[\chi_j^{3/2}(4.88 + T_e/\chi_j)],$$

$$\beta_{j,r} = 5.2 \times 10^{-14} j(\chi_j/T_e)^{1/2} \times [0.43 + 0.5\ln(\chi_j/T_e) + 0.47(\chi_j/T_e)^{1/3}],$$

$$\beta_{j,3b} = 2.97 \times 10^{-27}\,\xi_j/[T_e\chi_j^2(4.88 + T_e/\chi_j)].$$

Here n_j is the population density of ion species with atomic number Z in the charged state j (cm^{-3});
α_j is the recombination rate (cm^6/sec);
S_j is the collisional excitation rate (cm^6/sec);
$\beta_{j,r}$ is the radiative recombination rate (cm^6/sec);
$\beta_{j,3b}$ is the three-body recombination rate (cm^6/sec);
ξ_j is the number of outer-shell electrons;
χ_j is the ionization energy (eV) between charge state j and charge state $j + 1$; and
T_e is the electron temperature (eV).[6]

The power densities of continuum x rays brought about by bremsstrahlung (P_{ff}) and recombination radiation (P_{fb}) are obtained by solving the following expressions[7]:

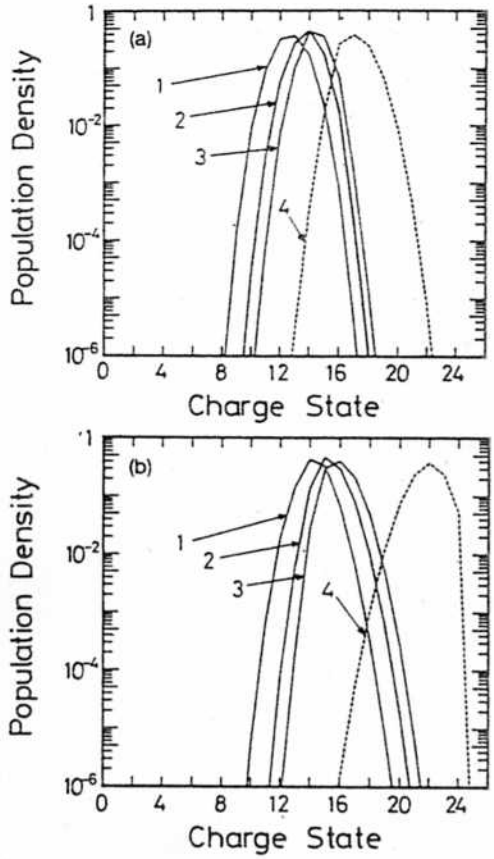

Fig. 5. Population densities of iron plasmas as a function of the charged state at different times and also in the steady state; 1: t = 10 psec, 2: t = 20 psec, 3: t = 30 psec, 4: in steady state. (a) T_e = 300 eV, (b) T_e = 700 eV.

$$P_{ff} = 1.5 \times 10^{-32} T_e^{1/2} n_e j^2 n_j,$$

$$P_{fb} = 1.5 \times 10^{-32} T_e^{1/2} n_e j^2 n_j (\chi_{j-1}/T_e).$$

In solving these equations, the following assumptions are adopted:

(1) The total population densities n_p ($= \Sigma_j n_j$) are assumed to have a constant value, because the effects of plasma expansion on the atomic processes are not so important within 30 psec of laser pulse width. The value of n_p is determined by the condition that n_e ($= \Sigma_j j f_j n_p$) becomes 10^{21} cm^{-3} at the end of the laser pulse.

(2) T_e is assumed to have a constant value throughout the ionization processes. In reality, T_e is changed spatially and temporally; however, this assumption is necessary to make analysis easier and to understand the genuine properties of x rays emitted from picosecond laser-produced plasmas. Calculations were performed for two iron plasmas with electron temperatures of 300 and 700 eV. These values were adopted by considering temperatures that were experimentally determined from measurements of x-ray continuum spectra. The curves shown in Fig. 5 indicate temporal changes of population densities computed at 10, 20, and 30 psec and also in the steady state, respectively.

Calculated x-ray spectra emitted from laser plasmas in the transient and steady states on the focal curve are

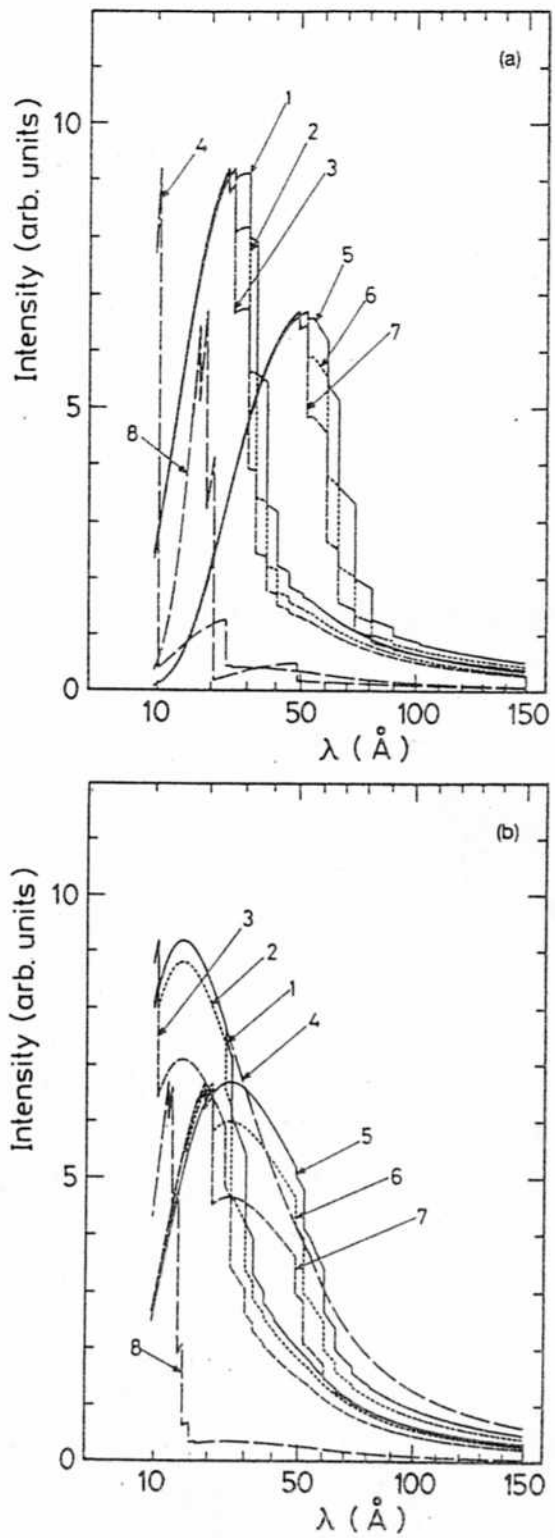

Fig. 6. First- and second-order x-ray spectra emitted from iron plasmas at different times and in the steady state. Curves 1–4 and 5–8 indicate first- and second-order x-ray spectra, respectively; 1,5: t = 10 psec; 2,6: t = 20 psec; 3,7: t = 30 psec; 4,8: in steady state. (a) T_e = 300 eV, (b) T_e = 700 eV.

shown in Fig. 6. These spectra can be obtained as a function of the position (x) on the focal curve: $I(x) = (dP_{ff}/d\nu + dP_{fb}/d\nu) \times d\nu/dx$. Curves 1–4 and 5–8 show

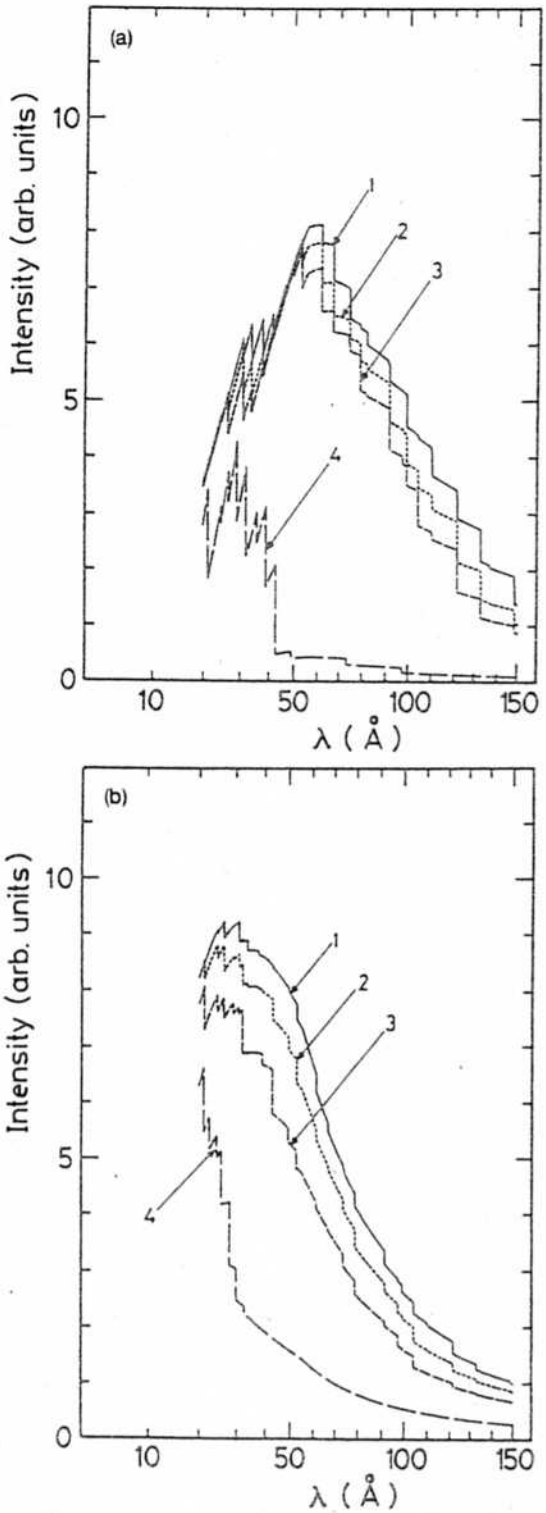

Fig. 7. X-ray spectra emitted from iron plasmas obtained by summing from first- to fourth-order reflected spectra assuming that higher-order components of x-ray spectra have the same reflectivity; 1: t = 10 psec, 2: t = 20 psec, 3: t = 30 psec, 4: in the steady state. (a) T_e = 300 eV, (b) T_e = 700 eV.

x-ray spectra reflected in first order and second order, respectively. First-order (second-order) x-ray spectra at 10, 20, and 30 psec denoted by curves labeled 1, 2 and 3 (5–7) are different from the x-ray spectrum simulated

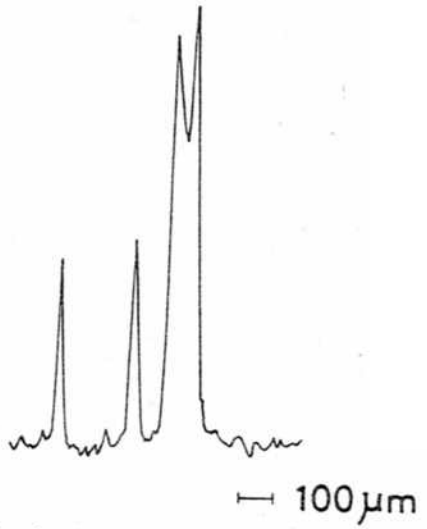

Fig. 8. Microdensitometer trace of a photographic plate near 100 Å obtained for aluminum plasmas shown in Fig. 3(b), which indicate a resolution of 0.09 Å and an energy resolution of 9.3×10^{-4}.

by assuming steady state, which is denoted by the curve labeled 4 (8). In reality, the measured reflected spectra are convoluted by higher-order components. Since reflectivity in the higher components is unknown, for simplicity this rate is assumed as equal throughout the higher-order components; the computed results summed from first- to fourth-order reflected spectra are shown in Fig. 7 to evaluate the effect due to these higher-order components.

IV. Discussions

A. Spectral Resolution

Figure 8 shows a microdensitometer trace (aperture 10 μm) near 100 Å for a spectrum from the aluminum plasmas in Fig. 3(a). From this result, the resolution of x-ray lines can be estimated. A halfwidth line was estimated as 15 μm on the photographic plate; this leads to a spectral resolution of 0.09 Å and an energy resolution of 9.3×10^{-4} ($\Delta E/E$). Precise measurements of the same spectra on the photographic plate with a microscope support this result, and the size of the x-ray emission region was simply estimated as 5.4 μm. If a laser-plasma image is transferred and focused on the entrance slit by a toroidal mirror, the spatial resolution will be improved up to a theoretical value. From the theoretical curves representing resolutions as functions of the x-ray wavelengths shown in Fig. 9, the resolution estimated for 100-Å x rays has a minimum value of ~7 μm in the best focal condition. This value corresponds to energy resolution 4.3×10^{-4} of $\Delta E/E$. These spectra were obtained with the entrance slit wide open (larger than 200 μm), so that it is better to treat the plasma source position as the light source of the spectrometer. The flat-field focal property is not so sensitive with the distance shift of the light source from the grating; however, coma-type aberration increases ~20 μm in 20-mm increments. The diameter of the emitting region of the laser plasmas is much smaller than 100 μm,

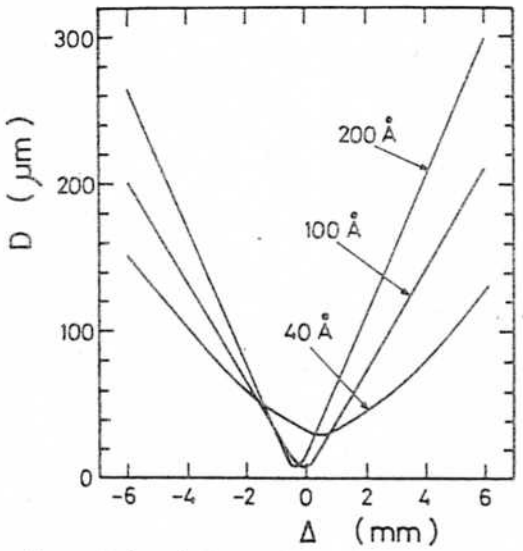

Fig. 9. Theoretical resolution evaluated at different wavelengths as a function of distance from the focal curve.

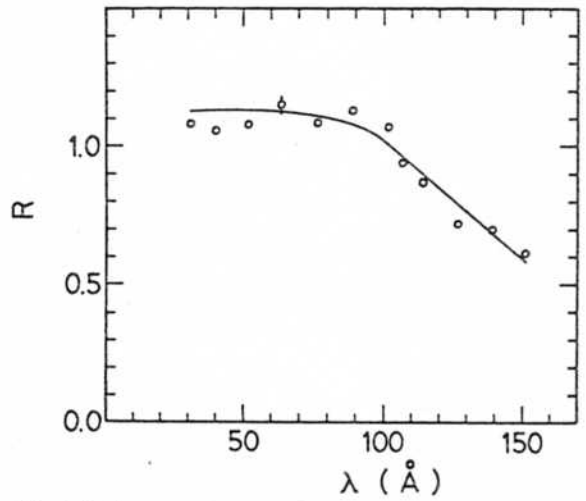

Fig. 10. Relative x-ray intensity ratio between the results for a 2400-grooves/mm grating and a 1200-grooves/mm grating.

which was estimated with the results of optical shadowgraphs. The 5.4-μm estimated value seems reasonable because the x-ray emitting region is restricted to high-density and high-temperature plasmas located near the critical surface, the size of which is estimated as less than several microns. The ruling errors and the imperfection of the blank surface of the grating is negligible. The limiting factors of spectral resolution with this spectrometer are mainly the higher-order aberration of spectral images caused by the alignment errors of the optical system and the size of the light source.

B. Detection Limit of the Spectrometer Toward Shorter Wavelengths

X-ray lines emitted from aluminum plasmas [1 and 2 in Fig. 3(b)] are identified as $1s^2 3p\ ^2P_0$—$1s^2 2s\ ^2S$ (48.3 Å) and $1s^2 3s\ ^2S$—$1s^2 2p\ ^2P$ (54.4 Å) in lithium-like ions, respectively. In this photograph, the x-ray lines located near 8 Å cannot be observed (measured by a spectrometer equipped with a KAP crystal.[3] X-ray line emissions from iron plasmas [3 in Fig. 3(b)] originate from Fe XVII and XVIII ions due to transitions between $3d$ and $2p$ levels. These lines cause emissions at wavelengths near 15 Å as reported in Ref. 8. In the result obtained with the 1200-grooves/mm grating, these lines are located out of focus in the focal curve of Fig. 2(a); they are positioned near the zero-order reflection and the SNR is then degraded. It is concluded that the short-wavelength limit is extended to 15 Å by the 2400-grooves/mm grating from 40 Å for carbon plasmas already reported in Ref. 2 by using the 1200-grooves/mm grating.

C. Comparison of Reflectivities Between a 1200-grooves/mm Grating and a 2400-grooves/mm Grating

Figure 10 shows the ratio between the x-ray intensity obtained by a 1200-grooves/mm grating (I_1) and by a 2400-grooves/mm grating (I_2) as functions of wavelength. The reflectivity of the 2400-grooves/mm grating is decreased as the wavelength increases above 100 Å. The reason for this decrease cannot be explained just by reflectivity of the gold coating on the grating, since reflectivity of gold increases with increasing wavelength and incident angle. Typically, it takes 90% for 44.6 Å and 114 Å for an incident angle of 89°; with an incident angle of 87° it is kept at 90% for 114 Å whereas it decreases to 70% for 44.6 Å.[9] The decrease in the reflectivity ratio originates from the grating characteristics which are mainly determined by the blazed wavelengths.

D. Comparison Between Experimental and Computational Results of X-Ray Spectra

Since reflectivity ratios for higher-order reflected spectra are not made clear as a function of wavelength and since in the experiments the spectra were obtained by accumulating signals from 100 shots, it is difficult to quantitatively discuss the comparison between experimentally obtained x-ray spectra and those computed. The effect of contributions from higher-order reflected spectra can be understood from Fig. 7, which was obtained when the ratio of reflectivities is assumed to be equal and the intensities of reflected x rays are added from first order to fourth order. As described in Sec. III the experimental results of x-ray spectra are different from those in the steady state, as shown in Figs. 6 and 7. However, the functional dependence of observed spectra can be qualitatively explained by those in transient state for 300 and 700 eV of T_e. In addition, we suggest that transient solutions are essential for giving the correct explanation of the experimental results. Since x-ray line radiations from iron plasmas in charged states of 16 (Fe XVII) and 17 (Fe XVIII) are observed as shown in Fig. 3, it can be concluded that both charged states are generated to some extent. This agrees with charged states computed in the transient state represented by Figs. 5(a) and (b).

V. Conclusion

We have presented the development of a grazing-incidence flat-field XUV spectrometer using a grating with varied groove spacing.

We have shown various spectroscopic characteristics attained by this spectrometer. Studies of picosecond XUV spectroscopy were performed with this new type of spectrometer and it was shown that it has many advantages over a conventional instrument. Results are summarized as follows:

(1) We have demonstrated how clearly and easily XUV spectra are taken on a conventional photographic plate with reasonable resolution. Energy resolutions were estimated as 9.3×10^{-4} in the 100-Å region.

(2) According to our preliminary measurements, results of time-resolved XUV spectra will be performed by a combination of this spectrometer and the XUV streak camera with 10-psec time resolution which we have developed recently.

(3) XUV spectra from iron XVII, XVIII located at 15 Å are clearly measured and recorded on a flat photographic plate by using a 2400-grooves/mm grating. However, the XUV spectra emitted from aluminum located near 8 Å were not recorded (previously measured by a KAP crystal). Considering these facts, it is concluded that the detection limit toward shorter wavelengths was successfully extended to the 15 Å region. Efforts will be continued.

(4) We have carried out computations to analyze the transient characteristics of picosecond XUV radiations from picosecond laser-produced plasmas with special interest in the dynamic atomic processes.

As a result, drastic changes were found in the simulated picosecond XUV spectra computed by assuming steady-state conditions. We demonstrated the importance of the transient treatment in analyzing XUV spectra emitted in ultrashort time durations. Thus, it now becomes possible to predict characteristics of XUV and x-ray pulses generated from picosecond laser-produced plasmas. Our studies should be useful not only for spectroscopic studies in the XUV regions relevant to x-ray laser or other physics but also for other applications such as x-ray lithography and diffractions in biological studies.

References

1. R. J. Fonck, A. T. Ramsey, and R. V. Yelle, "Multichannel Grazing-Incidence Spectrometer for Plasma Impurity Diagnosis: SPRED," Appl. Opt. **21**, 2115 (1982).
2. T. Kita, T. Harada, N. Nakano, and H. Kuroda, "Mechanically Ruled Aberration-Corrected Concave Gratings for a Flat-Field Grazing-Incidence Spectrograph," Appl. Opt. **22**, 512 (1983).
3. N. Nakano and H. Kuroda, "X-ray Generation from Laser-Produced Plasmas and Its Atomic-Number Dependence," Phys. Rev. A **27**, 2168 (1983).
4. N. Nakano, M. Nagase, Y. Tanaka, and H. Kuroda, in *Laser Interaction and Related Plasma Phenomena, Vol. 6*, H. Hora and G. H. Mily, Eds. (Plenum, New York, 1984), p. 14.
5. T. Harada and T. Kita, "Mechanically Ruled Aberration-Corrected Concave Gratings," Appl. Opt. **19**, 3987 (1980).
6. D. Colombant and G. F. Tonon, "X-ray Emission in Laser-Produced Plasmas," J. Appl. Phys. **44**, 3524 (1973).
7. D. Mosher, "Coronal Equilibrium of High-Atomic-Number Plasmas," Phys. Rev. A **10**, 2330 (1974).
8. L. F. Chase, W. C. Jordan, J. D. Perez, and R. R. Johnston, "X-ray Spectrum of a Laser-Produced Iron Plasma," Phys. Rev. A **13**, 1497 (1976).
9. J. A. R. Samson, *Techniques of Vacuum Ultraviolet Spectroscopy* (Wiley, New York, 1967).

The authors would like to express their sincere thanks to T. Namioka of Tohoku University and S. Shionoya of Tokyo University for helpful discussions concerning this work.